14. FRACTURING, ALTERATION, AND PERMEABILITY: *IN-SITU* PROPERTIES IN HOLE 735B[1]

D. Goldberg,[2] C. Broglia,[2] and K. Becker[3]

ABSTRACT

Geophysical logs recorded over 500 m in Hole 735B have been analyzed to identify the *in-situ* properties and the fracture permeability of basement rocks in the Atlantis II Fracture Zone. Although hydroxyl-bearing alteration minerals were found to be most abundant in the upper section of this hole, the highest permeabilities were also measured in this zone by packer tests. This interval corresponds to the presence of several open fractures imaged by the acoustic televiewer and to indications of fluid flow through transmissive fractures in the log responses. Negative temperature-gradient and large semblance anomalies were found to correlate well with the largest of the observed fracture zones near 40, 100–150, 200, and 264 mbsf. Although no stress-induced wellbore breakouts were observed in the televiewer images, most of the 70 identified fractures strike subparallel to the north-south fracture zone and dip steeply west-southwest. These fractures probably formed as a result of normal faulting on the transform side of the uplifted ridge, where Hole 735B was sited in the Atlantis II Fracture Zone, rather than as a direct result of horizontal plate-tectonic motion.

INTRODUCTION

During Leg 118 of the Ocean Drilling Program, scientists on board the *JOIDES Resolution* drilled into crystalline rocks in the vicinity of the Atlantis II Fracture Zone near the Southwest Indian Ridge. This fracture zone is one of a series of north- to south-trending transform faults that offset the slow-spreading Southwest Indian Ridge (Fig. 1). Site 735 is located to the east of the Atlantis II Fracture Zone on a platform lying in 731 m of water. The position of the platform in the magnetic anomaly pattern on the transform wall suggests a crustal age of about 12 Ma (Robinson, Von Herzen, et al., 1989). As the gabbro was emplaced high on the flank of the fracture zone, it was probably subjected to stress, which resulted in a variety of deformational textures and fractures.

Hole 735B was drilled to a depth of 500 mbsf and penetrated primarily gabbro, as described in detail by the shipboard scientific party (Robinson, Von Herzen, et al., 1989). A complete suite of in-hole electrical, acoustic, and nuclear logs and hydraulic packer tests were recorded. The overall recovery of core was 87%, and below 100 mbsf, recovery was 95%; thus, Hole 735B gave the first nearly continuous recovery of core in fresh and altered oceanic gabbro. This study focuses on the processing and interpretation of the downhole data, in particular, the Schlumberger neutron porosity log, the acoustic borehole televiewer log, the multichannel sonic log, the borehole temperature profile, and four hydraulic packer tests. Direct comparison of the core with the extensive suite of downhole logging measurements provides characterization, for the first time, of the *in-situ* physical properties of oceanic gabbro and their relationships to tectonics and hydrogeology at this fracture zone site.

DOWNHOLE MEASUREMENTS

Alteration and Porosity Profile

The Schlumberger neutron porosity tool used in Hole 735B employs a chemical source of AmBe to bombard the formation with fast neutrons and four detectors to measure their concentration in epithermal (>0.2 eV) and thermal (<0.025 eV) energy ranges (Ellis et al., 1988). During the scattering process, the neutrons interact elastically with nuclei in the formation, losing part of their kinetic energy with each collision; eventually, they are reduced to the thermal energy level at which they can be absorbed by the surrounding nuclei. Because its mass is equal to that of a neutron, the hydrogen atom is most efficient in slowing down neutrons. The slowing-down length, L_s, is the average distance a neutron must travel to reach the thermal energy level, usually between 10 and 30 cm (McKeon and Scott, 1988). This parameter depends largely on the concentration of hydrogen in the rock, and also on the relative concentration of its other constituents, and thus is different for basalts and for most sedimentary rocks.

However, most rocks also contain hydrogen in the form of bound water associated with clays and other alteration minerals. Broglia and Ellis (1990) have presented in detail the technique necessary to correct the neutron porosity measured in basaltic and gabbroic rocks for the presence of hydrous minerals. In Figure 2, the apparent porosities of basaltic samples, computed from L_s, are plotted as a function of their hydrogen weight fraction measured by X-ray analysis (after Broglia and Ellis, 1990). The apparent porosity of basalts that contain no water-filled porosity and only bound hydrogen ranges from 1% in fresh massive units to about 35% in highly altered units. The positive linear relationship implies that apparent neutron log porosity may exceed the value of the water-filled porosity, if hydrous minerals are among the rock constituents. Hence, basaltic rocks that have undergone extensive alteration in the form of hydrous clay mineralization (e.g., celadonite, palagonite, amphiboles, talc, zeolites, and iron-hydroxides) will exhibit elevated apparent porosities by an amount linearly related to their contents of bound water. Gabbro, having the same elemental composition as basalt, is assumed to have a similar neutron log response. With this relationship established, shipboard X-ray measurements of the hydrogen weight fraction on core samples from Hole 735B

[1] Von Herzen, R. P., Robinson, P. T., et al., 1991. *Proc. ODP, Sci. Results*, 118: College Station, TX (Ocean Drilling Program)
[2] Borehole Research Group, Lamont-Doherty Geological Observatory, Palisades, NY 10964 U.S.A.
[3] Rosenstiel School of Marine and Atmos. Science, University of Miami, FL 33149 U.S.A.

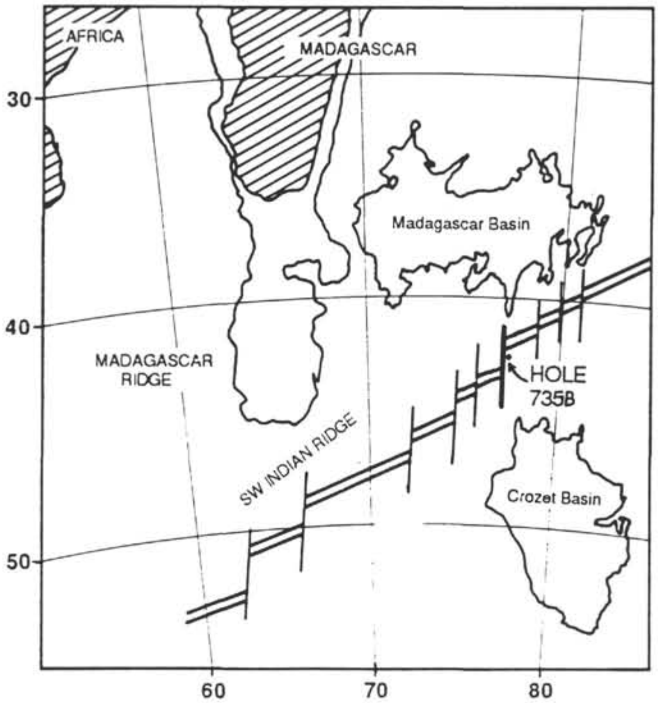

Figure 1. Location map of Hole 735B in the Atlantis II Fracture Zone.

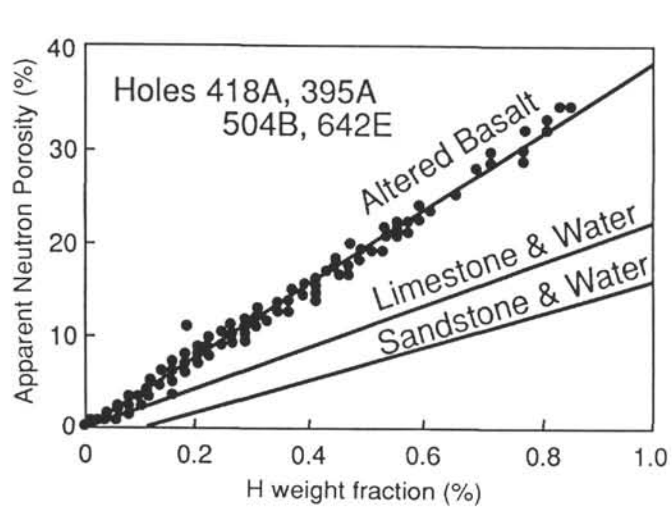

Figure 2. The linear relationship between computed apparent porosity and hydrogen content at four DSDP-ODP Sites (after Broglia and Ellis, 1990). The apparent neutron porosity of altered basalts exceeds the values of the water-filled porosity by an amount related to the bound-water content. This relationship has been used in Hole 735B to estimate the neutron response to hydrous minerals from the H weight fraction of selected samples (also see Fig. 5, track 3).

were used to estimate directly the effect of bound hydrogen on the neutron log response (Fig. 3, track 2, dots).

Estimates from core, however, do not provide a continuous profile of bound water, such as is traditionally obtained from the gamma-ray log in sedimentary formations (Poupon and Gaymard, 1970). Furthermore, the gamma rays in Hole 735B have a low signature because amphiboles, the major hydrous mineral present in the gabbros, lack potassium. Therefore, to predict continuously the effect of bound hydrogen on the neutron log, alternative logs that are sensitive to the alteration minerals present must be used (Broglia and Ellis, 1990). The hydrogen yield log recorded with the induced gamma-ray spectrometry tool, a pulsed-neutron device that measures the relative concentration of some of the rock constituents (Hertzog et al., 1987), was chosen as a continuous measure of hydrous alteration in Hole 735B. In the absence of large changes in borehole size (see caliper and density log correction in Fig. 3, track 6), both the hydrogen yield and neutron porosity logs measure the concentration of hydrogen in formation pores and hydroxyls bound in alteration minerals. The correlation between the hydrogen yield and the neutron logs indicates that both are sensitive to the same parameters. Differences between them may be attributed to increases in the hydrogen yield response from seawater in the borehole or from the sensitivity of the measurement to certain heavy elements, such as titanium, in the formation.

A continous alteration estimate was computed by re-scaling the mean hydrogen yield (Fig. 3, track 3) to match the hydrogen weight fraction measurements of core samples (Fig. 3, track 2, dots). The re-scaled curve (Fig. 3, track 2, line) roughly represents the response of the neutron log to hydrous alteration minerals. This continuous curve then can be used to correct the neutron log for the porosity effect of the bound hydrogen. The corrected porosity, ϕ_c, is computed simply by

$$\phi_c = \phi_l - \phi_a,$$

where ϕ_l and ϕ_a are the original neutron log and the re-scaled hydrogen yield log, respectively. ϕ_c and ϕ_l logs and core-derived porosities are plotted in Figure 3 (track 1). Clearly, the minimum ϕ_c values correspond reasonably well with the core-derived values; peaks may be attributed to fracture porosity unsampled by coring.

An estimate of the volume of alteration V_{alt} can be computed from ϕ_a by

$$V_{alt} = \phi_a/\phi_m,$$

where $\phi_m = 16\%$ is the neutron response to actinolite-tremolite amphiboles (Ellis et al., 1988). In Figure 3, the volume of alteration estimated from the logs (track 3) compares on average with the results from shipboard core-sample modal analyses (track 4). The correlation of ϕ_c and V_{alt} with other data is discussed below.

Acoustic Borehole Televiewer

The borehole televiewer is an ultrasonic device that is used to image the wall of a borehole, producing information about the distribution and orientation of natural and induced features intersecting the hole. A piezoelectric transducer mounted on a central shaft emits a focused 3° beam while rotating 3 times per second..An 0.4-MHz pulse is transmitted into the borehole fluid at 600 regular intervals per revolution, each time reflecting from the wall of the borehole and returning to the transducer for reception. The full analog signal, returned to the surface through a standard wireline logging cable, is recorded on videotape. A fluxgate magnetometer in the downhole instrument produces a north orientation pulse, which is recorded along with the analog signals. The mechanical operation of the acoustic borehole televiewer is described fully by Zemanek et al. (1970).

Digitization of the recorded signals allows for extraction of peak amplitude and traveltime information of the borehole-reflected waveforms. Image processing improves the data and can produce both unwrapped-borehole amplitude and traveltime displays over selected depth intervals or wireframe cylindrical projections (Barton, 1988). We used such process-

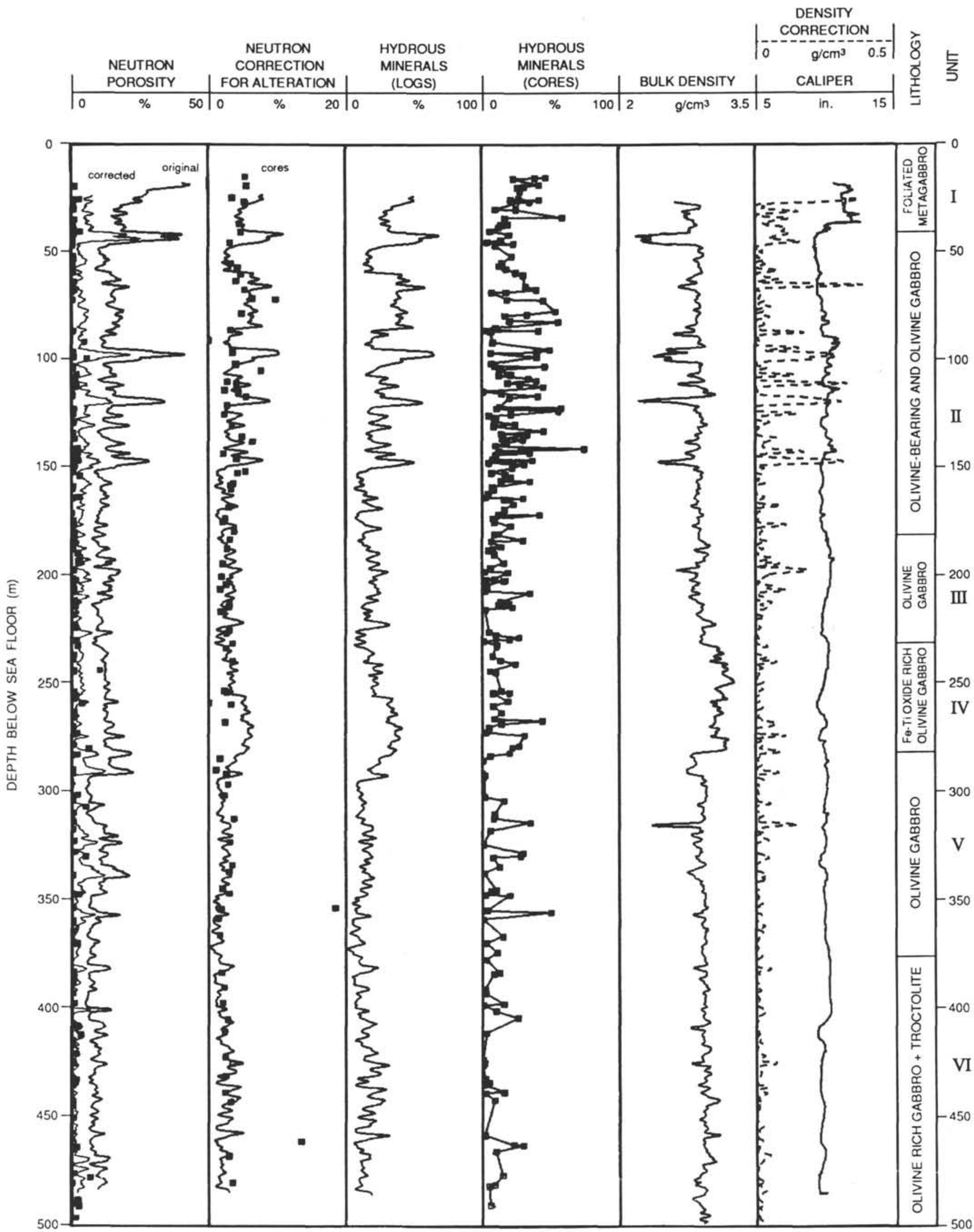

Figure 3. Porosity and alteration profiles at Hole 735B (tracks 1 through 4). Also displayed are the capture cross section and bulk density (track 5), and caliper and density correction (track 6). Locally, the alteration can be as high as 60%, which corresponds to a neutron porosity correction of about 10%. Differences between log and core porosities are attributed to the presence of open fractures. Alteration and porosity decrease downhole, and the olivine-rich gabbros and troctolite layers in the lower part of the hole exhibit porosities of less than 2%.

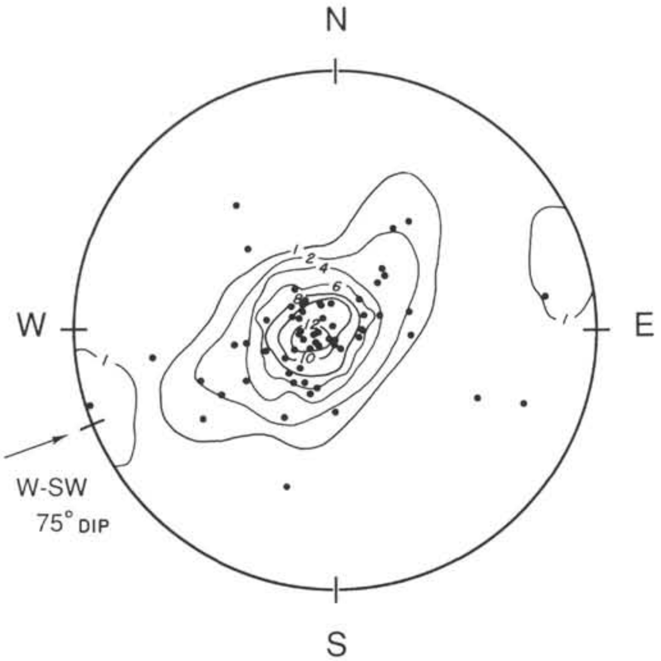

Figure 4. Lower hemisphere plot of fracture dips computed from televiewer image analysis. Contours indicate the frequency of occurrence (number) of fractures in equant circles of about 1/5 the radius of the stereonet. The centroid of the distribution dips approximately 75° W-SW. Fracturing is likely to have resulted from uplift of the walls of the Atlantis II Fracture Zone, not horizontal plate tectonic motion.

ing to determine the location and orientation of fractures intersecting the wellbore with superior resolution to other logging tools. Ideally, televiewer images can resolve open fractures as fine as 0.5 cm in a water-filled borehole. The televiewer can also provide an accurate measurement of the diameter, surface roughness, and ellipticity of the borehole.

One geometrical technique used to obtain the orientation of planar features intersecting the wellbore involves peak-to-trough analysis of the sinusoidal trace of features on an unwrapped amplitude or traveltime image (Zemanek et al., 1970). The strike of a feature is given by the azimuthal orientation of the midpoint between peak and trough; the dip is calculated by the arc tangent of the height (peak-to-trough) divided by the borehole diameter. Depending on the logging speed, a minimum horizontal dip of about 20° can be resolved from an unwrapped image. Features that do not affect either the roughness, reflectivity, or radius of the borehole cannot be resolved at all.

Over the 500-m interval logged in Hole 735B, geometrical analysis of televiewer amplitude images identified 70 fractures having measurable strikes, dips, and apparent apertures (see Appendix). Figure 4 shows the dip vector of each fracture plotted on an equal-area, lower-hemisphere stereonet. The number of fractures in equant circles of about one-fifth the radius of the stereonet is shown by the contours (after Seeberger and Zoback, 1982). The centroid of the entire fracture distribution indicates a north-northwest strike and a west-southwest 75° dip. Analysis of the fractures in smaller depth intervals shows no distinct trends in orientation with depth.

Unfortunately, no wellbore breakouts were observed in the televiewer data that allow for direct measurement of the minimum horizontal stress direction. As proposed by tectonic models of the Atlantis II Fracture Zone, significant uplift of the eastern transform wall, where Hole 735B was sited, occurred after a readjustment of north-south tectonic-plate motion and induced extension across the transform valley (Dick et al., this volume). Most probably the *in-situ* fracturing is the result of normal faulting on the transform side of this uplifted ridge, subparallel to the transform, rather than a direct result of horizontal plate motion.

The mechanical and hydrological characteristics of a fracture are controlled primarily by the degree of contact of its walls and the size of the resulting permeable pathways (Brown and Scholz, 1985). In lieu of a better measurement, the width of fractures measured by the borehole televiewer as they intersect the wellbore, their "apparent aperture," may be used as an estimate of these characteristics (Barton, 1988; Barton and Moos, 1988). The apparent aperture of a fracture in a televiewer image differs from the true fracture width as a result of fracture dip and borehole geometry effects, wall destruction and fluid injection during drilling, and dispersion of the acoustic televiewer beam. Even after correcting for geometric effects, the apparent aperture is only a rough estimate of true fracture width and probably does not indicate transmissivity through rock away from the borehole walls. For the purposes of this rough estimation, the apparent apertures of fractures in Hole 735B were measured with an attainable resolution of about 2 cm from unwrapped amplitude images. A log of the cumulative fracture aperture over 2-m intervals is displayed in Figure 5 (track 5). Although the mean cumulative aperture in the hole is less than 2 cm, its greatest value (28 cm) is reached near 40 mbsf due to a large concentration of small fractures. Elsewhere, large-aperture (2–8 cm) intervals generally result from single fractures, and consequently, the fracture density more or less mirrors the cumulative aperture log.

As seen in other studies of fracturing in crystalline rock wells, there is an overall decreasing trend in fracture aperture and fracture density with depth (Seeberger and Zoback, 1982; Haimson and Doe, 1983). This is expected for subhorizontal fractures that close gradually with increasing overburden pressure. In this shallow hole, however, many fractures are high-angle and remain open with depth, an expected result from steep block uplift. In addition, subsequent hydrothermal alteration may fill fractures at certain depths. The correlation of the fracture distribution with the other logs in this hole is discussed below.

Multichannel Sonic Log

A multichannel sonic (MCS) logging tool, configured similarly to the geometry of a surface refraction survey, has a source separated from an array of hydrophone receivers suspended in a borehole. Acoustic energy from the source travels as a compressional pulse in the borehole fluid and converts at the borehole wall into a series of body- and guided-wave modes. The velocities and amplitudes of compressional and shear body waves are primarily a function of the formation properties. The guided modes are controlled by the properties of both the formation and the fluid-filled borehole (e.g,. Cheng and Toksoz, 1981). Shear waves are most influenced by high-amplitude guided modes at nearby frequencies, and direct V_s measurements are usually contaminated (e.g., Paillet and White, 1982). These V_p and V_s estimates, however, can be used to characterize the elastic properties of the formation (Goldberg and Gant, 1988).

The MCS tool used in Hole 735B has a single source located 2 m above a 12-receiver array. The array spans 1.65 m, and both the source and the array are centered in the borehole by means of bowstring centralizers. Full waveforms are transmitted from each of the receivers through a standard logging cable and are digitally recorded uphole. In this hole,

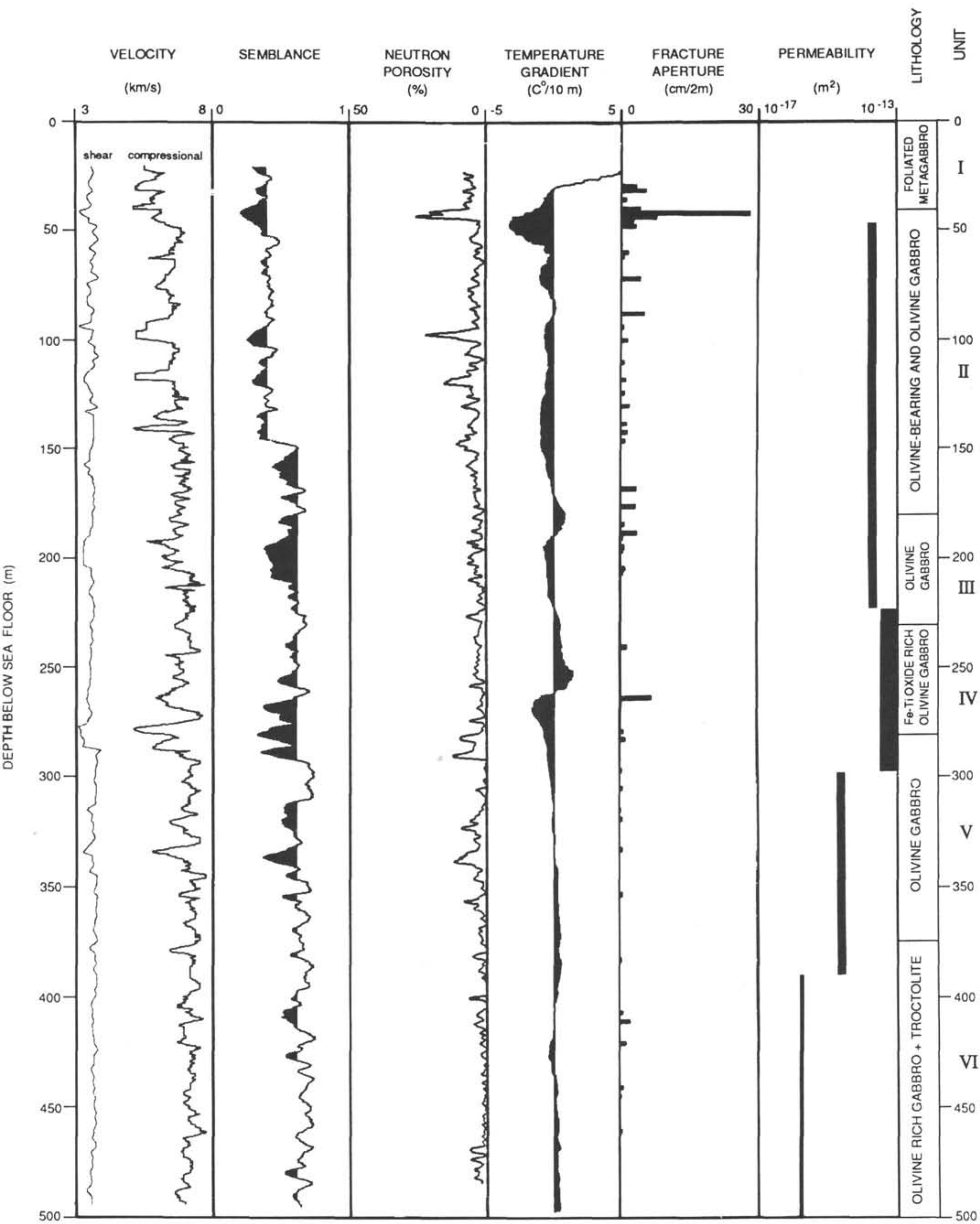

Figure 5. Geophysical logs in Hole 735B: V_p and V_s, (track 1), mean semblance (track 2), corrected neutron porosity (track 3), temperature gradient (track 4), 2-m cumulative fracture aperture (track 5), and bulk permeability (track 6). Mean semblance (shaded below the mean) changes systematically at 150 mbsf due to a malfunction of the pre-set receiver gains. Uncertainty in permeability estimates is represented by the line width. As indicated by low-velocity and low-semblance, high-porosity, and negative temperature-gradient perturbations, large fractures identified at 40 and 264 mbsf contribute most to the measured permeability.

the source was fired at 30-cm intervals, producing nearly 20,000 waveforms in less than 3 hr over the 500-m depth interval.

The complete waveform acoustic data were analyzed to yield compressional and shear velocities across the receiver spread using a modified semblance calculation (Kimball and Marzetta, 1984). Semblance was applied here as a measure of the coherence between channels to calculate the compressional and shear group velocities across the receiver array and as a normalized measure of the amplitudes of these waves. At Site 735, the MCS waveforms required pre-processing to remove unwanted noise and the guided-wave modes from the signal. Time domain filters were used to remove noise outside the principal 2.5- to 17.5-kHz frequency band of the signal. In addition, an electronic malfunction precluded computer control for data acquisition in the upper 140 m, and waveforms were not recorded in their usual increasing-offset sequence with pre-set gains. A pre-semblance process to reorder the sequence of recordings by threshold picking of the high-amplitude fluid arrival was designed to return the data to sequential order. The data were then processed normally for velocities by semblance correlation of waveforms having increasing moveout.

The compressional (V_p) and shear (V_s) velocities and their mean semblance in Hole 735B are displayed in Figure 5 (tracks 1 and 2, respectively). V_p shows considerable variation throughout the hole and averages 6.7 ± 0.3 km/s. Overall, V_p agrees well with ultrasonic measurements performed in the laboratory (Itierrino et al., this volume) and with vertical seismic profiling results in this hole (Swift et al., this volume). V_s is generally less variable than V_p because of the strong influence of guided modes, but is representative of the average V_s in the hole (3.5 ± 0.15 km/s). V_p/V_s and Poisson's ratio thus are reliable only for large interval averages and are not shown.

Several low V_p zones occur throughout the hole (e.g., 40, 90, 120, and 140 mbsf, etc.), and nearly all correspond with semblance anomalies (shaded below the mean) and elevated porosities. The mean semblance is broadly lower in the upper 140 mbsf, where the pre-set gain of waveform was disabled. The correlation of the V_p and semblance logs with porosity, alteration, and fracturing will be discussed below.

Borehole Temperature Profile

High-precision temperature logs (within 0.01°C) were run before and after the completion of the other logging experiments in Hole 735B (Robinson, Von Herzen, et al., 1989). A temperature-gradient profile was computed by spatial differencing of the temperature log over 10-m depth intervals. In Figure 5 (track 4), the temperature-gradient profile shows negative gradient anomalies from 30–50, 65–70, 90–160, 190–210, 260–270, and 430 mbsf. The repeat temperature profile indicates that the borehole cooled about 1.5°C overall during the 38-hr logging period, but maintained the temperature-gradient anomalies. An extrapolation of the temperature log to equilibrium was computed by Von Herzen and Scott (this volume) and also shows that the temperature-gradient anomalies remain present at depth.

In dense crystalline rocks, fluid flow is likely to occur through fractures, which shifts the temperature profile and yields an anomalously low or negative temperature gradient. Here, negative gradient anomalies occur over intervals containing fractures, although not all of the observed fractures correspond to negative gradient anomalies. Negative gradient anomalies cannot be caused by variations in thermal conductivity with depth, because all earth materials have conductivities greater than zero. Consequently, the observed negative gradient anomalies in this hole result from the presence of transmissive fractures that contribute cool fluid back into the borehole, which was displaced by warm bottom water during drilling or which originated from a connected fluid source (Von Herzen and Scott, this volume). During packer tests, probably the same transmissive fractures that influenced the temperature profile are hydraulically active.

Hydraulic Testing

An inflatable, single-element, drill-string packer was used to measure the average *in-situ* transmissivities and to calculate the average permeabilities of four different intervals isolated in Hole 735B: 49–500, 223–500, 299–500, and 389–500 mbsf. These intervals correspond to the zones between the bottom of the hole and the depths at which the packer was inflated. The packer inflation depths were chosen to isolate the major lithologic units, which also exhibited a different character in the downhole logs. Thus, the inflation at 389 mbsf isolated lithologic Unit VI, the inflation at 299 mbsf isolated Units V and VI, the inflation at 223 mbsf isolated Units III through VI, and the inflation at 49 mbsf isolated Units II through VI.

As described in detail by Becker (this volume), these measurements were performed either by monitoring the decays of nearly instantaneous pressure pulses applied to the isolated zone ("slug tests") or by monitoring the gradual pressure increases as seawater was pumped at a constant rate into the isolated zone for up to 30 min (injection tests). These are standard techniques, which yield the bulk transmissivities and permeabilities of the respective isolated zones with accuracies of about ± 30% (for slug tests see Bredehoeft and Papadopulos, 1980; for injection tests see Matthews and Russell, 1967; for further processing details see Becker, this volume).

Results show that permeability decreases by more than two orders of magnitude in the deepest 200 m of Hole 735B. As the quality of data was good, the permeabilities of the smaller overlapping intervals (e.g., 49–223, 223–299, and 299–389 mbsf) could be estimated by taking the differences in transmissivities measured in the isolated zones. These interval permeabilities are plotted in Figure 5 (track 6), and both the measured and calculated interval permeabilities are summarized in Table 1. The relationship of these measurements with other logging data is interpreted below to determine the influence of alteration and fracturing on the *in-situ* permeability.

DISCUSSION

Fracturing, Alteration, and Permeability

The variation of *in-situ* permeability with depth in Hole 735B suggests that certain intervals are hydraulically transmissive and others are tight. To differentiate these intervals, subdivisions of Hole 735B, based on the average porosity, volume of alteration, and fracture aperture logs, were compared with the measured interval permeability (Table 2 and Fig. 5). We found that subdivisions based on the log responses correspond nearly, but not exactly, to the lithologic units (Units I through VI) described in Robinson, Von Herzen, et al. (1990). Differences can be largely attributed to fracturing, which is not accurately represented in the recovered core. We also found that the weak correlation of *in-situ* permeability with porosity and its strong correlation with temperature and televiewer logs gives evidence that fracturing controls the measured permeability in Hole 735B.

The upper 150 m of Hole 735B, most of Units I and II, are characterized by 32.2% average alteration volume and an average porosity of 5.6%. Core values in this interval average 23.4% alteration by volume and 1.7% porosity. In this most highly altered interval, the presence of open fractures, which

Table 1. Measured and calculated hydraulic transmissivity and permeability over various depth intervals in Hole 735B (after Becker, this volume).

	Interval (mbsf)	Transmissivity (10^{-6} m^2/s)	Permeability (10^{-15} m^2)
Measured:	49–500	54	24
	223–500	32	24
	299–500	2.0	2.1
	389–500	0.1	0.2
Calculated:	49–223	22	24
	223–299	30	81
	299–389	1.9	4.4

Table 2. Mean and (standard deviation) of log and core measurements over various depth intervals and lithologic units in Hole 735B.

Lith. unit	Interval (mbsf)	Porosity (%) log	Porosity (%) core	Alteration volume (%) log	Alteration volume (%) core
I/II	23–150	5.6 (4.7)	1.7 (1.2)	32.2 (13.3)	23.4 (15.4)
II/III	150–230	3.4 (2.0)	1.5 (0.7)	16.6 (6.5)	13.5 (9.7)
IIV	230–280	2.6 (1.7)	2.4 (1.8)	26.9 (9.0)	15.2 (10.0)
V	280–375	3.4 (3.1)	1.5 (1.3)	13.6 (6.9)	11.4 (12.3)
VI	375–500	1.7 (1.8)	1.5 (1.0)	14.3 (6.6)	8.2 (8.2)

were not measured in laboratory core samples, can account for the core vs. log discrepancy. In addition, the caliper and the density correction logs (Fig. 3, track 6) tend to show spikes in intervals where hole diameter varies sharply due to fracturing. In the interval from 150 to 230 mbsf, made up of Units II and III, the volume of hydrous alteration minerals decreases dramatically to averages of about 16.6% and 13.5% from logs and cores, respectively. While the core porosity is similar to that determined for the interval above, the average log porosity is 3.4%, suggesting that one or more open fractures affect the log response. From the seafloor to 230 mbsf, the corrected porosity is anomalously high, as expected, where isolated, water-filled fractures were observed in the televiewer log (Fig. 5, tracks 4 and 5). The permeability is high in this interval, 24×10^{-15} m^2, indicating that one or more fractures are conductive even though alteration minerals are abundant (Fig. 5, track 6). However, if the hydrologic structure of the site does not change dramatically, hydrothermal mineralization of the remaining open fractures probably will continue to reduce this high permeability.

The interval from 230 to 280 mbsf, spanning the Fe-Ti oxide gabbro identified as Unit IV, is differentiated from the rocks above by an increase in the average alteration volume measured on cores (26.9%) and from the logs (15.2%), but displays the highest interval permeability, 81×10^{-15} m^2, determined from the packer tests (Fig. 5, tracks 3 and 6). The televiewer log in this zone indicates that it contains a few small fractures near 290 mbsf and a wide-aperture, high-angle fracture at 264 mbsf, shown by a cylindrical wireframe projection in Figure 6. The dip of this fracture is 72° west-southwest, and the apparent aperture is about 8 cm. Because of the associated thermal anomaly at this depth, this fracture probably is contributing most to the measured permeability in the interval. Note that the abundance of dense, magnetic Fe-Ti oxides below 260 mbsf in Unit IV affects the north orientation pulse of the televiewer and results in horizontal offsets of up to 30° in the image of this fracture.

The olivine gabbro in Unit V is distinguished by a small increase in average log porosity to 3.4% and a large decrease in permeability to 4.4×10^{-15} m^2 (see Tables 1 and 2). At 375 mbsf, the Unit VI olivine gabbros and troctolites have even lower average log porosity (1.7%) and permeability (0.2×10^{-15} m^2). The volume of alteration in these two units remains nearly constant and is the lowest in the hole. Core and log porosities also agree well in both Units V and VI, indicating a minimal effect of unsampled fractures, and only a few high-porosity anomalies occur at depths where small-aperture fractures were observed in the televiewer log (Fig. 5, tracks 3 and 5).

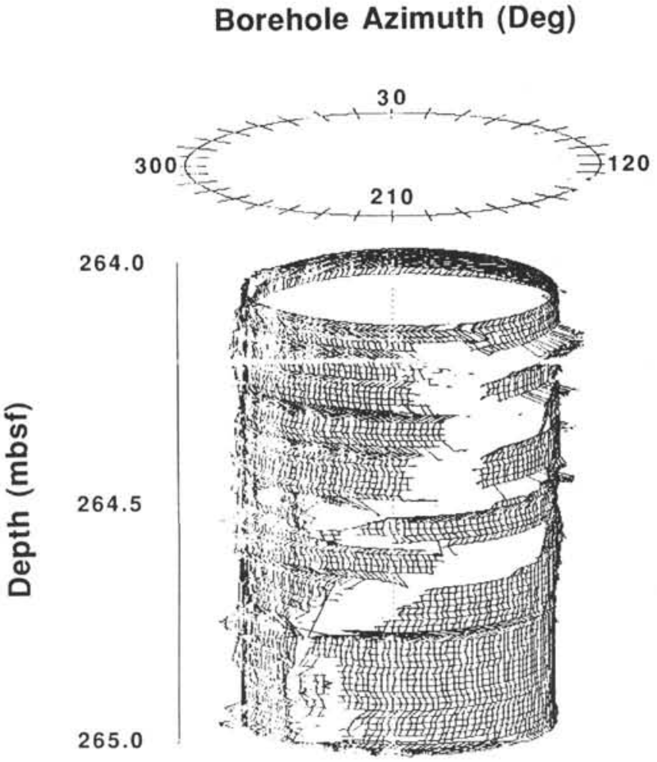

Figure 6. Cylindrical wireframe projection of a high-angle (72° W-SW), wide-aperture (8 cm) fracture near 264 mbsf. Horizontal offsets in the image of this fracture resulted from misorientation of the north synchronization pulse of the borehole televiewer by strong remanent magnetization in this Fe-Ti oxide-rich zone.

Downhole Logs as Permeability Indicators

Indicators of fracturing from downhole experiments (e.g., acoustic, porosity, temperature, and televiewer logs) may be used to distinguish fractures that are transmissive from those that are not. For example, the causal relationship between fluid flow through fractures and negative temperature-gradient anomalies probably indicates which transmissive fractures contribute cool fluid back into the borehole. As shown in Figure 5 (tracks 4, 5, and 6), negative gradient anomalies occur in Units I through IV at depths where the porosity is high, fractures are observed, and the measured permeability is high. The magnitude of the temperature-gradient anomalies also shows a general correlation to fracture aperture. Because the temperature gradient in a borehole is assumed to be affected by fluid flow through even a small open fracture, the gradient log effectively indicates depths at which fractures are transmissive, but smoothes their response over a wider interval. It is likely that depths where the negative gradient anomalies are greatest, specifically near 40 and 264 mbsf, are near multiple or large open fractures, which contribute most to fluid flow in this hole.

In a similar manner, acoustic properties, particularly guided-wave amplitudes, have been related to hydraulic transmissivity in previous studies of fractured rocks (e.g., Paillet, 1980; Hardin et al., 1987; Barton and Moos, 1988). Such correlations result from measurable decreases in signal amplitude from elastic and inelastic dissipation across impedance boundaries and porous fractures. Reasonable mechanisms controlling this effect may result from a combination of changes in Poisson's ratio, scattering and interference, and dissipation by formation and borehole fluid movements. Observations suggest that velocity and semblance also decrease as a result of these mechanisms (e.g., Moos and Zoback, 1983; Goldberg and Gant, 1988). Ideally, with constant lithology and borehole size, decreases in velocity and semblance could be attributed largely to the effects of fractures and correlated to their transmissivity.

Because acoustic logs can achieve greater depth resolution than hydraulic or temperature measurements, they are useful for detailed correlation of fracture transmissivity to the measured permeability. In Hole 735B, fracture occurrences generally correspond to zones of high porosity, low V_p and low semblance (Fig. 5; tracks 1, 2, 3, and 5). In most of these zones, V_p anomalies correspond with the fracture location, but without a clear relationship to fracture aperture. Semblance anomalies, however, occur at depths where large fracture apertures and negative temperature-gradient anomalies are spatially coincident, notably at 40, 100–150, 200, and 264 mbsf, as well as over several other depth intervals. These coincident anomalies may be the best indicators about which fractures intersecting the borehole are transmissive, because both reflect the result of fluid movement through fractures by independent physical measurements.

CONCLUSIONS

From our interpretation of the geophysical logs recorded in these oceanic layer 3 gabbros, we were able to conclude the following about the *in-situ* properties of Hole 735B:

1. Although the greatest abundance of hydroxyl-bearing alteration minerals were observed in the upper section of the hole, the highest permeabilities also occur in this interval.
2. About 70 fractures were identified from the televiewer images, which strike predominantly north-northwest and dip steeply west-southwest, and no wellbore breakouts were observed.
3. Fracturing in Hole 735B is most likely the result of normal faulting on the transform side of the uplifted ridge on the eastern wall of the Atlantis II Fracture Zone, rather than a direct result of horizontal plate-tectonic motion.
4. Anomalies in the temperature gradient and mean semblance, and to a lesser extent in velocity and porosity, correspond to the cumulative fracture aperture log computed from televiewer images recorded in the hole.
5. Fracturing near 40, 100–150, 200, and 264 mbsf corresponds to large and coincident negative temperature-gradient and semblance anomalies that indicate active fluid flow and is consistent with high packer-test transmissivities measured in these intervals.

ACKNOWLEDGMENTS

D. Goldberg and C. Broglia were supported during this research by the National Science Foundation and Joint Oceanographic Institutions, Inc. under contract JOI 66-87D. K. Becker was supported by the National Science Foundation under contracts OCE 85-13537 and OCE 88-00077. The authors thank C. Wilkinson and C. Barton for their assistance with the televiewer image processing.

REFERENCES

Barton, C. A., 1988. Development of *in-situ* stress measurement techniques for deep drill holes [Ph.D. dissert.] Stanford Univ. Dept. of Geophysics.

Barton, C. A., and Moos, D., 1988. Analysis of macroscopic fractures in the Cajon Pass scientific drill hole: over the interval 1829-2115 meters. *Geophys. Res. Lett.*, 15:1013–1016.

Bredehoeft, J. D., and Papadopulos, I. S.,1980. A method for determining the hydraulic properties of tight formations. *Water Resources Res.*, 16:233–238.

Broglia, C., and Ellis, D., 1990. The effect of alteration, formation absorption, and standoff on the response of the thermal neutron porosity log in gabbros and basalts: examples from DSDP–ODP Sites. *J. Geophys. Res.*, 95:9171–9188.

Brown, S. R., and Scholz, C. H., 1985. Broad bandwidth study of the topography of natural rock surfaces. *J. Geophys. Res.*, 90:12,575–12,582.

Cheng, C. H., and Toksoz, M. N., 1981. Elastic wave propagation in a fluid-filled borehole and synthetic acoustic logs. *Geophysics*, 46:1042–1053.

Ellis, D. V., Flaum, C., McKeon, D., Scott, H., Serra, O., and Simmons, G., 1988. Mineral logging parameters: nuclear and acoustic. *The Technical Review*, Schlumberger Educational Services, Houston, 38–52.

Goldberg, D., and Gant, W. T., 1988. Shear-wave processing of sonic log waveforms in a limestone reservoir. *Geophysics*, 53:668–676.

Hardin, E. L., Cheng, C. H., Paillet, F. L., and Mendelson, J. D., 1987. Fracture characterization by means of attenuation and generation of tube waves in fractured crystalline rock at Mirror Lake, New Hampshire. *J. Geophys. Res.*, 92:7989–8006.

Haimson, B. C., and Doe, T. W., 1983. State of stress, permeability and fractures in Precambrian granite of northern Illinois. *J. Geophys. Res.*, 88:7355–7371.

Hertzog, R., Colson, L., Seeman, B., O'Brien, M., Scott, H., McKeon, D., Wraight, P., Grau, J., Ellis, D., Schweitzer, J., and Herron, M., 1987. Geochemical logging with spectrometry tools. *Soc. Pet. Eng. J.*, Pap. 16792.

Kimball, C. V., and Marzetta, T. L., 1984. Semblance processing of borehole acoustic array data. *Geophysics*, 39:587–606.

Matthews, C. S., and Russell, D. G., 1967. *Pressure Build-Up and Flow Tests in Wells*: Dallas (Soc. Pet. Eng. AIME), Monogr. 1.

McKeon, D. C., and Scott, H. D., 1988. SNUPAR-A nuclear parameter code for nuclear geophysics applications. *Nucl. Geophys.*, 2(4):215–230.

Moos, D., and Zoback, M. D., 1983. *In-situ* studies of velocity in fractured crystalline rocks. *J. Geophys. Res.*, 88:2345–2358. Paillet, F. L., 1980. Acoustic propagation in the vicinity of fractures which intersect a fluid- filled borehole. *Trans. SPWLA 21st Annu. Logging Symp., Pap.* D.

Paillet, F. L., and White, J. E., 1982. Acoustic modes of propagation in the borehole and their relationship to rock properties. *Geophysics*, 47:1215–1228.

Poupon, A., and Gaymard, R., 1970. The evaluation of clay content from logs. *Trans., SPWLA 11th Annu. Logging Symp., Pap.* G.

Robinson, P. T., Von Herzen, R. P., et al., 1989. Site 735. *In* Robinson, P. T., Von Herzen, R. P., *Proc. ODP, Init. Repts.*, 118: College Station, TX (Ocean Drilling Program), 89–816.

Seeberger, D. A., and Zoback, M. D., 1982. The distribution of uatural fractures and joints at depth in crystalline rock. *J. Geophys. Res.*, 87:5517–5534.

Zemanek, J., Glenn, E. E., Norton, L. J., and Caldwell, R. L., 1970. Formation evaluation by inspection with the borehole televiewer. *Geophysics*, 35:254–269.

Date of initial receipt: 12 July 1989
Date of acceptance: 4 May 1990
Ms 118B-144

APPENDIX

Tabulated depth, azimuth, and plunge (dip) of fracture dip vectors measured from borehole televiewer images in Hole 735B.

Depth (mbsf)	Azimuth (degrees)	Dip (degrees)	Depth (mbsf)	Azimuth (degrees)	Dip (degrees)
28.60	235.7	38.2	136.41	210.0	70.7
30.15	111.4	21.5	141.70	321.4	38.2
31.90	115.7	38.2	145.77	222.9	73.7
35.25	351.4	81.5	166.33	30.0	52.7
35.65	162.9	83.7	174.62	42.9	70.0
39.81	287.1	78.3	183.98	210.0	57.9
39.57	94.3	65.8	186.16	81.4	17.7
40.38	34.3	48.1	189.67	227.1	70.3
40.66	34.3	48.1	192.15	261.4	78.6
41.60	240.0	48.1	195.30	330.0	80.8
41.88	240.0	48.1	203.06	244.3	75.9
41.55	252.9	0.0	203.78	227.1	82.9
42.59	252.9	0.0	204.22	38.6	77.6
42.88	252.9	0.0	263.51	240.0	72.0
43.77	261.4	61.7	280.32	342.9	88.5
43.63	265.7	79.1	239.78	180.0	63.9
45.23	77.1	65.8	277.46	312.9	76.1
45.82	261.4	29.1	280.55	312.8	74.2
47.21	197.1	36.6	281.40	287.1	75.7
55.50	214.3	86.8	294.05	300.0	74.5
59.16	218.6	68.8	303.34	252.9	67.3
60.56	330.0	81.2	313.11	257.1	83.1
60.72	107.1	82.0	315.26	180.0	85.2
70.57	261.4	57.8	317.21	308.6	76.4
86.20	201.4	68.3	317.74	231.4	80.2
87.92	240.0	57.6	327.32	278.6	68.1
92.99	197.1	70.7	347.92	304.3	84.6
98.07	248.6	43.6	351.95	300.0	78.3
108.40	38.6	65.6	380.62	72.9	75.1
116.16	64.3	79.7	404.41	278.6	68.2
117.93	235.7	82.8	408.32	278.6	68.2
122.40	184.3	81.0	418.69	252.9	79.7
123.93	201.4	72.4	442.27	90.0	81.3
128.98	42.9	66.8	439.13	175.7	86.7
129.24	312.9	52.3	458.04	261.4	84.8